The Influence of Pressure on Flame-Flow Characteristics of a Reacting Jet in Crossflow

Michelle Otero
University of Central Florida
12781 Ara Dr, Orlando FL, 32828
Michelleotero@knights.ucf.edu
ASME Member

Tommy Genova Jr.
University of Central Florida
12781 Ara Dr, Orlando FL, 32828
Tommy.genova@knights.ucf.edu
ASME Member

Bernhard Stiehl
University of Central Florida
12781 Ara Dr, Orlando FL, 32828
Bernhard.Stiehl@knights.ucf.edu
ASME Member

Anthony J. Morales
University of Central Florida
12781 Ara Dr, Orlando FL, 32828
Selaroma627@knights.ucf.edu
ASME Member

Scott Martin
Embry-Riddle Aeronautical University
1 Aerospace Blvd, Daytona Beach, FL 32114
Martis38@erau.edu
ASME Professional Member

Kareem A. Ahmed[1]
University of Central Florida
12781 Ara Dr, Orlando FL, 32828
Kareem.ahmed@ucf.edu
ASME Professional Member

[1] Corresponding author: Kareem Ahmed, Email: Kareem.ahmed@ucf.edu.

Abstract

This work experimentally investigates the effects of elevated combustor pressures on the characteristics of a lean premixed reacting methane/air jet injected into a lean vitiated crossflow using a 12.7mm axial jet. Experiments were conducted in an axially staged combustor, which implements a reacting jet in crossflow (RJIC) configuration and operates over a pressure range of 1 to 5 atmospheres. Simultaneous CH chemiluminescence and Particle Image Velocimetry (PIV) are used to study the flow field and flame behavior. The results show that the reacting jet trajectory exhibits greater penetration with elevated pressure, which is a novel finding compared to available data in the literature. However, the flame lift-off point and ignition delay time both decreased with elevated pressure, which was attributed to decreased vorticity along the flame boundary which corresponds to increased Damköhler numbers (Da). Emissions measurements confirm the NO_x increase with pressure as reported in the literature for single stage gas turbine combustors. Concurrently, emission measurements for the staged configuration show the strong NO_x benefit of the RJIC system: the data proves a reduction of global outlet emission levels at elevated pressure with the axially staged configuration. The axial emission reduction was attributed to the decreasing lift-off at elevated pressure levels. Hence, the research emphasizes that the flame and emission characteristics are coupled; they are not only dependent on the geometric parameters and momentum flux ratios but are also a function of pressure.*

Keywords: Reacting jet in crossflow, flame stabilization, flame liftoff, vorticity

1. INTRODUCTION

Today's power generation industry demands low cost, high efficiency, reliable, and clean burning gas turbines that meet governmental emission policies. To meet these demands, researchers and original equipment manufacturers (OEM) are continuously integrating novel engineering designs to achieve higher turbine firing temperatures and lower NOx emissions over a wide load range [1–5]. The efficiency of gas turbine combustors was previously limited by many design factors; however, improvements to thermal coatings, turbine cooling strategies, and premixing of reactant mixtures have led to the development of Dry Low NOx (DLN) combustors, which can withstand elevated firing temperatures for improved efficiency. The present issue with current DLN combustors is achieving the required firing temperature in order to reach the desirable increased efficiency, while effectively limiting NOx emissions. NOx formation occurs via a reaction mechanism known as the extended Zeldovich mechanism [6, 7]. The rate of NO production is proportionally related to residence time and temperature. Despite technological advancements, additional research is required to promote enhanced strategies to overcome NOx emission and its dependency on temperature and residence time [8–13]. Axial staging is a promising technique to reduce NOx, as it lowers the residence time of high temperature products while simultaneously reducing the excess oxygen molecules after reaction by separating the combustion process between two stages [14–16]. In axial staging combustion, the bulk of the reactant is ignited at lean conditions in the first stage to minimize the temperature of combustion products and mitigate thermal NOx formation. Prior to the combustor outlet, the remaining reactant mixture is injected into the vitiated products through Jet in Crossflow (JIC). By injecting and combusting close to the inlet of

the turbine, the desired high temperatures are obtainable with shorter residence times, thus reducing NOx production. As such, a thorough understanding of the structural, mixing, and reactive flow characteristics is essential to determine optimum operating conditions and improve control strategies. Due to this, the Jet in Crossflow field has been investigated by the scientific community for decades. Non-reacting JIC correlations have been established in a variety of published work, relating to jet trajectories [17–19], velocity profiles [20, 21], and vorticial structures [22–24]. Majority of the non-reacting JIC correlations are all derived as a function of the momentum flux ratio *J*, given by Eq. (1).

$$\boldsymbol{J = \frac{\rho_j u_j^2}{\rho_\infty u_\infty^2}} \tag{1}$$

Velocity and density are denoted by u and ρ, with subscripts ∞ and j differentiating crossflow and jet parameters, respectively. Current trajectory models utilize a power law function, shown in Eq. (2). The x and y coordinates represent the stream-wise and transverse direction and are nondimensionalized by the momentum flux ratio (J) and the diameter of the injector (d). The coefficients A and B vary based on the non-reacting JIC experimental studies. Coefficient A represents the entrainment of the crossflow fluid and the range is $1.2<A<2.6$; meanwhile coefficient B is the shape constant and has a range of $0.28<B<0.34$ [18, 25–28].

$$\boldsymbol{\frac{y}{\sqrt{J}d} = A\left(\frac{x}{\sqrt{J}d}\right)^B} \tag{2}$$

Nevertheless, knowledge on the behavior of RJIC under vitiated crossflow is limited [29–33], with studies including flame stabilization, jet penetration, NO_x production and

flame structures [34–36]. This limited knowledge on the topic has sparked an interest in further investigation during recent years. Lamont et al [37] focused on investigating premixed jets in addition to diffusion and non-reacting jets. From the results, Holdeman correlations [20] adequately describe the trajectory of the JIC for fuel-only injection. However, for the premixed injection, the Holdeman correlation trajectory provides a poor match. The discrepancy can be explained by the higher local heat release provided by the premixed reacting jet. The additional heat release effectively increases the momentum of the jet, making it less susceptible to the crossflow mechanical forces than a non-reacting jet.

An initial approach for a lift-off height model for a premixed jet in vitiated crossflow was presented by Kolb et al [38]. The experiment investigated the effects of equivalence ratio, jet preheat temperature, crossflow temperature and momentum ratio on the flame lift-off height. The study came to various conclusions: (1) the turbulent time scale associated with higher jet velocities influences the flame liftoff height, (2) the influence of the chemical time scale is stronger than the influence of the turbulent time scale, (3) at the higher temperatures, both the chemical time scale and the ignition delay time is shorter, influencing the liftoff height, and finally (4) the flame liftoff height decreases due to the higher reactivity of the mixture and the lower chemical time scales associated to higher jet equivalence ratio. Wagner et al [39] studied the flow-field and flame stabilization of a premixed RJIC system, consisting of a premixed ethylene-air jet injected into a lean vitiated crossflow with high lateral confinement. The findings showed the windward flame stabilization to be highly dependent on the jet and crossflow mixing, where the heat transfer between the crossflow and jet led to autoignition. The research suggested the windward

flame stabilization mechanism to be autoignition-assisted propagation, a similar behavior as seen in non-premixed RJIC systems. Strain rate probability density functions (pdfs) indicated a high correlation between the local strain rate and leeward flame stabilization location. Furthermore, confinement was found to have a significant impact on both the non-reacting and reacting jet trajectory. At the lower momentum flux ratios J<15.7, the reacting jet penetrated further into the crossflow compared to its non-reacting counterpart, which was attributed to the increase in velocity, leading to high dilatation rates. Ebi et al [40] characterized the transient ignition process leading to a stable flame in the secondary stage in an axial stage combustor. The finding insinuated that the ignition process had a dependency on the ignition timescale ratio, defined as the ratio between the autoignition time and the combustor timescale. At a timescale ratio of less than 1, the ignition process was dominated by autoignition. During autoignition, there was a continuous stream of large kernels emanating from the vitiated crossflow that ignite and stabilize the axial jet flame as soon as the fuel was injected into the flow. With timescale ratios greater than 1, the dominate ignition process fell into the propagation regime.

For industry applications, jet-in-crossflow research is focused on parameters that drive NOx in axially staged turbine combustors [41–46]. A recent study from Sirignano et al [47] investigated NOx formation sensitivity to axial temperature rise, jet momentum flux ratio and equivalence ratio in an effort to determine their sensitivity to NOx formation. Sirignano et al injected a rich premixed reacting jet into a vitiated crossflow, varying one parameter at a time. This work revealed that NOx production was controlled by the jet equivalence ratio, the flame stabilization and the mixing between crossflow and jet products. In addition, a new parameter, the flame liftoff, was seen to influence NOx production. This

parameter was shown to be highly impacted by the equivalence ratio of both the crossflow and the axial jet. From the results, the correlations showed that as the flame liftoff distance increased, the NOx emissions decreased.

In summary, the current literature studying RJIC has increased our understanding of the key physical parameters driving flame-flow behavior and NOx formation. However, it has provided limited insight to the gas turbine community. Most of the previous experimental work has been conducted at atmospheric conditions, whereas operating pressure conditions in gas turbines range from 20 to 30 atm, depending on the design. Pressure and temperature are known as influential properties affecting the flow field, flame stabilization and propagation dynamics, as well as emission production [48–51]. The lack of research on premixed reacting jet in crossflow at elevated pressure has led to this work, which experimentally investigates flame-flow characteristics of a RJIC configuration over a range of combustor pressures. The novelty of the research is that the experiment allows for a range of combustor pressures to be investigated (1-5 atm) while maintaining all other relevant parameters constant (such as J and ΔT). Thus, the influence of pressure on key flame-flow physics can be isolated.

2. EXPERIMENT AND DIAGNOSTICS

2.1. Experimental Facility

The experiments in this study were performed using the high pressure RJIC combustor facility at the Propulsion and Energy Research Laboratory, located at the University of Central Florida (UCF). The facility is comprised of three main sub-assemblies, the main burner stage, a mixing section, and the axial stage, as shown in Fig. 1.

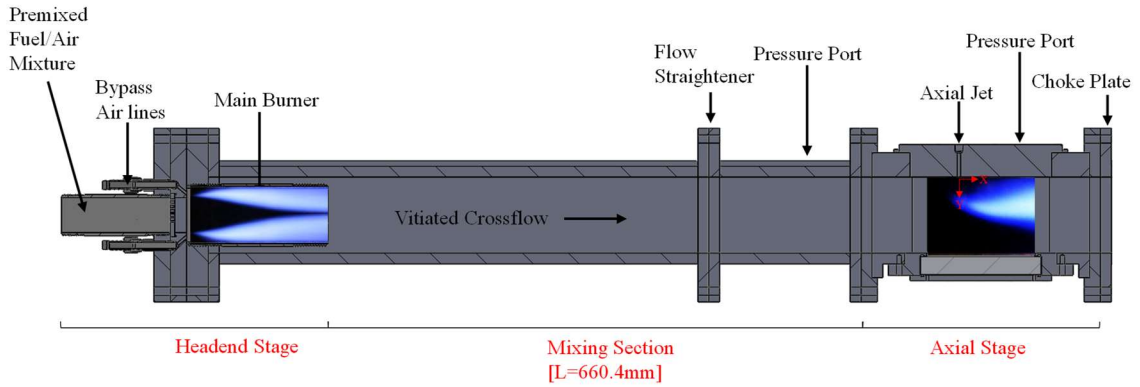

Fig. 1: High-pressure Reacting Jet in Crossflow (RJIC) facility.

The main combustion zone, referred to as the main burner stage in axial staged combustion systems, provides the high temperature vitiated crossflow, composed of products from a lean methane/air mixture. In this facility, high-pressure compressed air is supplied and regulated to the required pressure upstream of a restricted orifice union (ROU) to obtain the desired air mass flow rates for main stage combustion. Methane is distributed into the flow downstream from the air ROU through a choke orifice and modulated upstream of the orifice. The premixed mixture is injected into the main burner and stabilized with a backward facing step flame holder. It consists of a 38.1 mm diameter stainless steel pipe expanding to a 63.5 mm diameter pipe. The height difference provides a step size of 10 mm, where the recirculation zone is formed.

To control the main burner equivalence ratio and remaining oxygen percentage, additional air is supplied around the main burner, using four 6.35 mm diameter bypass air lines, which are equally positioned circumferentially. In addition, the bypass air lines assist with cooling along the walls as the vitiated flow enters the test section downstream. Further stabilization of the flame is achieved using hydrogen pilot lines, located circumferentially around the main burner. The supplementary hydrogen lines have a diameter of 3.175 mm,

providing minimal amount of hydrogen throughout the duration of the run to assist in flame stabilization. Prior to entering the test section, the burnt products of the main stage flow through the mixing section, which includes a 54% open area perforated plate prior to entering the test section.

The test section has a rectangular cross-sectional area of 76.2 mm x 88.8 mm and a choked exit diameter of 38.1 mm. The axial stage (referred to as the secondary stage) consist of the test section housing the axial jet injector. The stainless-steel test section is designed with a 12.7 mm top plate and three quartz viewing windows located at the bottom, right, and left side of the test section. Multiple viewing windows allow for maximum optical access capabilities for laser diagnostics measurements. The axial jet flow is injected through an orifice (d_j = 12.7 mm), which is flush to the upper wall of the test section and located 144 mm from the exit of the mixing section. The system is run remotely using a series of automatic pneumatic actuators and solenoid valves controlled by a NI LabVIEW VI. Dwyer pressure transducers are located throughout the facility to acquire pressure readings at a sampling frequency of 350Hz. For temperature measurements, a ceramic insulated with exposed bead type B thermocouple is located between the mixing section and the test section to obtain flow temperature entering the secondary stage.

2.2. Optical Diagnostics and Processing Techniques

Simultaneous CH* chemiluminescence and Particle Image Velocimetry (PIV) systems captured the reacting jet in crossflow behavior. An overview of the diagnostics setup can be seen in Fig. 2.

The Particle Image Velocimetry of the reacting axial jet was taken to obtain quantitative information of the flow field. Images were acquired with an Andor Zyla 5.5 camera, coupled with an Evergreen 200 Dual Nd:YAG 532 nm laser (100 mJ at 25Hz). The laser is operated in a frame-straddling mode, where each laser head is independently pulsed at 25 Hz with a time delay of 20 μs between pulse pairs. The 532 nm beam exiting the dual pulse laser was focused down with a f1000 Plano convex cylindrical lens. 76.2 mm downstream from the first lens is a f-12.7 Plano concave cylindrical lens to produce the laser sheet. The sheet is then reflected upwards towards the bottom glass of the test section with a 45° mirror. Imaging was attained at a resolution of 2160 x 2560 pixels (1 pixel = 0.04 mm) and a rate of 25 frames per second. The Andor camera is mounted perpendicular to the laser sheet and is equipped with a 50 mm NIKKOR lens and a 532 nm narrow band filter. The camera and laser were controlled and synchronized through a BNC model 575 delay generator. 3 μm aluminum oxide particles were injected into the crossflow and axial jet prior the RJIC to capture the full flow-field. The crossflow was seeded through an in-line seeder located in the bypass air lines, while seed for the axial jet originated from an external seeder. 12% of the total axial air was rerouted to the external seeder and redirected to the axial fuel/air mixture upstream of the jet injector on the test section.

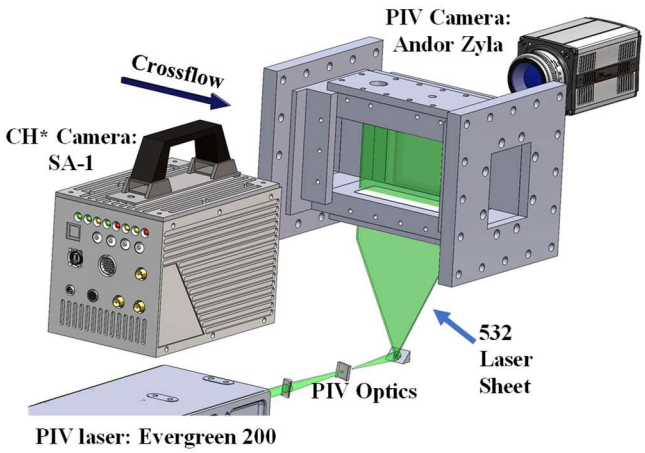

Fig. 2: Experimental setup for simultaneous PIV and CH* Chemiluminescence diagnostics.

PIV Mie scattering images were processed using MATLAB PIVlab 2.02 software. A region of interest (ROI) within the image was chosen to eliminate light reflection from the test section walls. Images were then preprocessed with a contrast limited adaptive histogram equalization [CLAHE] technique to improve the contrast in the image. Vector processing was done using a four step multi-pass Fast Fourier Transform (FFT) window deformation method, initialing with an interrogation window of 128 x 128 pixels, and reducing to a region of 16 x 16 pixels with a 50% overlap throughout all interrogation windows, resulting in a vector resolution of 600 μm/vector. The associated uncertainly from the PIVlab correlation is 0.02 pixels, corresponding to ±0.045 m/s [52].

Flame visualization was attained with CH* chemiluminescence, using a Photron SA-1 monochrome high-speed camera. A 430 nm narrowband filter with high transmissibility was mounted to the camera, permitting for only the axial jet CH* excited wavelength to transmit to the camera. Images were captured simultaneously with the PIV at a rate of 125 frames per second and a shutter speed of 1/1000. Imaging of the region of interest was obtained with a resolution of 768 x 768 pixels (1 pixel = 0.21 mm) and focused on the jet center plane within the test section.

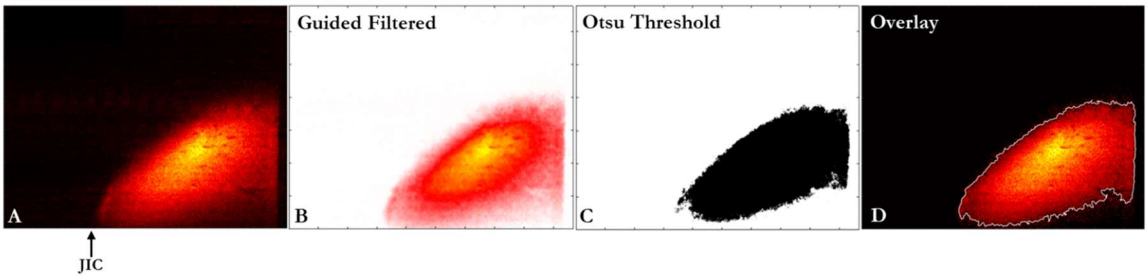

Fig. 3: Flame edge processing: (a) contour time average chemiluminescence image, (b) filtered image with background noise subtraction, (c) binarized flame edge threshold using Otsu method, (d) resulting flam edge overlay on contour image.

The flame boundary is determined using the CH* images, which highlight the heat release regions of the flame. To extract the flame edges and trajectory, an image processing technique was applied to the instantaneous images, allowing to differentiate the flame brush from the background. A guided image filter [53] is first applied to the raw images to eliminate background noise, and all images are then normalized by their highest intensity, as shown in Figs. 3a and 3b. The sequence of filtered images is then time-averaged to identify the mean flame brush. The exact flame coordinates are attained through Otsu's method [54], finding the minimal intra-class variance between two clusters of pixels: a foreground and a background cluster, with the foreground being the bright region of the flame in this study, as shown in Fig. 3c. The mean flame brush is overlaid onto the CH* contour in Fig. 3d.

The extent to which the jet penetrates the crossflow can be described by the mean jet trajectory. For this study, the jet trajectory was defined in two ways: (1) the geometric center of the heat release region (determined from the CH* images) [55] and (2) the central streamline extending from the jet injection point (based on PIV data). For the first method, the trajectory was determined from the midpoint between the windward $\overline{\zeta_w(x)}$ and leeward $\overline{\zeta_l(x)}$ flame coordinates, obtained in the time-averaged CH* chemiluminescence data.

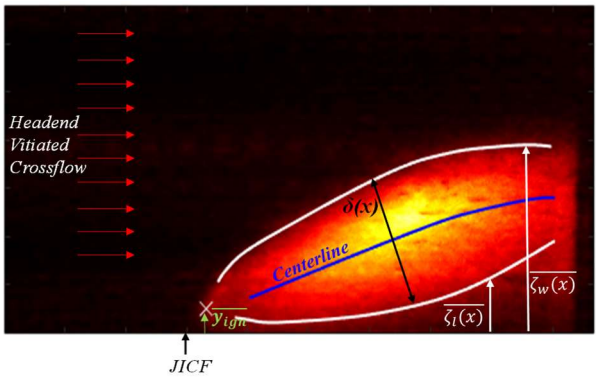

Fig. 4: Contour of time-averaged CH* chemiluminescence of reacting jet at 3 atm: centerline trajectory depicted in blue, time-average windward and leeward edges are shown as white lines. The white cross represents the ignition point and the jet width (δ) is represented with the black line. The origin of the coordinate system is placed at the jet injection location.

The time averaged flame coordinates were computed as the summation of the instantaneous CH* imaging threshold, divided by the total number of images. Referring to Fig 4., the white outer lines represent the average windward ($\overline{\zeta_w(x)}$) and leeward ($\overline{\zeta_l(x)}$) edge of the flame, and a blue line reflecting the centerline. The second method utilizes the average velocity magnitude field obtained from the PIV data, allowing to isolate the average streamline closest to the center of the jet exit to determine the trajectory.

2.3. Test Matrix

The conditions in this study were designed to investigate the influence of pressure on the flame/flow behavior of a reacting jet in crossflow system. To isolate the effects of pressure, all flow conditions were kept constant between cases. The vitiated crossflow was held at an equivalence ratio of Φ = 0.58 and an average velocity of 72 m/s. The total mass flow rate was varied with increasing pressure to account for density changes.

Table 1: Experimental test conditions.

Pressure [atm]	1	2	3	4	5
Crossflow Temperature [K]	1620	1620	1620	1620	1620
Crossflow Velocity [m/s]	72	72	72	72	72
Crossflow $Re_c = \frac{ud_h}{\upsilon}$	20,100	40,200	60,300	80,400	100,500
Jet Equivalence Ratio Φ	0.75	0.75	0.75	0.75	0.75
Jet Velocity [m/s]	87	87	87	87	87
Jet $Re_j = \frac{ud_j}{\upsilon}$	68,300	136,900	207,800	275,100	347,200
Momentum flux ratio J	8.9	8.9	8.9	8.9	8.9
Exit Temperature [K]	1667	1667	1667	1667	1667

For the axial jet, the equivalence ratio of each case was held at Φ = 0.75 with a velocity of 87 m/s. These conditions provided a global exit equivalence ratio of Φ = 0.60, which corresponds to a temperature of 1667 K. The temperatures were measured near the exit of the test section to ensure constant temperature between the cases. The crossflow Reynolds number ranged from 20,000 – 100,000 with a hydraulic crossflow diameter of 0.048 m, and the jet Reynolds number ranged from 68,000 – 350,000 with a jet diameter of 12.7 mm. The momentum flux ratio for all cases was $J = 8.9$, which was chosen for its industry relevance aspect. Mirroring operational load conditions, 15% of the total fuel mass was reallocated to the axial jet from the main burner. The total mass flow of the system was split between the main burner, the bypass air lines and the axial jet with a 73%, 15% and 12% fraction, respectively. The normalized vitiated crossflow velocity profile and turbulence intensity at various pressures were obtained, as shown in Fig. 5. With the onset of pressure, the normalized velocity profiles exhibit minimal change of the incoming crossflow prior to their interaction with the axial jet.

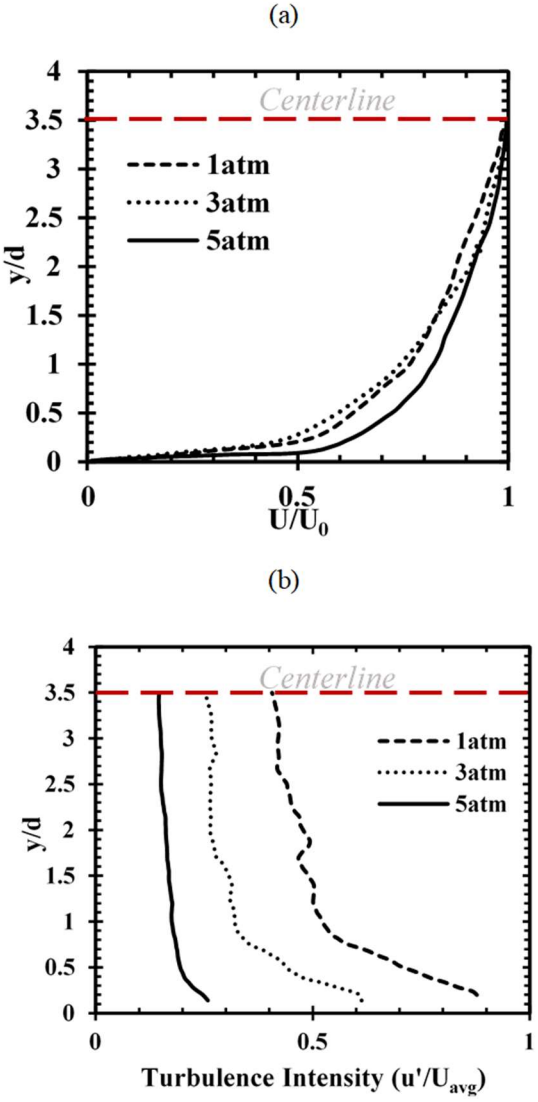

Fig. 5: Time averaged crossflow velocity and turbulence intensity profiles for P = 1, 3, and 5 atm. (a) Normalized velocity profile (U/ U_0) of vitiated crossflow at various pressures. (b) Turbulence intensity profiles (u'_{RMS}/U_{avg}).

3. RESULTS AND DISCUSSION

The following sections characterize the effect of pressure on the reacting jet in vitiated crossflow. The main behaviors investigated include flame and flow field trajectories, flame dispersion, flame liftoff heights, ignition timescale and flow field dynamics.

3.1. Reacting Jet Trajectories

The reacting jet trajectories determined from the CH* method are provided in Fig. 6a (solid lines). When comparing the 1-4 atm cases, the reacting jets follow similar trajectories for $x/d < 3$ downstream of the axial jet, which can be attributed mostly to the lifted flame behavior seen for all cases. The trajectories begin to deviate at $x/d > 3$, showing the higher-pressure reacting jets to penetrate slightly further into the crossflow. A larger variation is noticed for the 5 atm case, which significantly over-penetrates the other conditions. For example, at $x/d = 6.5$, an increase in pressure from 1 to 2 atm results in a 4.4% increase in the penetration depth (y/d). In comparison, increasing the pressure from 4 to 5 atm increases the penetration depth by 14.8%. Additional jet trajectories obtained with the PIV method (dashed lines) are also provided for the 1, 3 and 5 atm cases, as shown in Fig. 6. Similar penetration behaviors are noticed, i.e. the penetration depth at x/d = 6.5 from 1 to 5 atm increased by 28% for the CH* trajectory in comparison to an increase of 27% for the PIV trajectory. These slight differences are attributed to the nature of the measurements, such that CH* is a line-of-sight technique, whereas PIV provides planar measurement. Since the PIV-based trajectories track the velocity gradient along the shear layer, a higher amount of curvature was obtained relative to the CH*-based trajectories, which track the jet penetration based on the line-of-sight species concentration.

The PIV jet trajectories of the 1 and 5 atm cases are compared to commonly used literature correlations for non-reacting JICF (yellow line) [56, 57] and a RJICF correlation (red line) [39], as shown in Fig. 6b. The corresponding JICF correlations are provided in Eq. (2), where A and B are constants that vary between correlations. A large discrepancy is noticed between existing JICF correlations and the present data. These discrepancies can be attributed to the low momentum flux, high density ratio, and elevated pressures used in this study to explore conditions which are more relevant to axially staged gas turbines. The RJIC correlation equation is shown in Eq. (3)

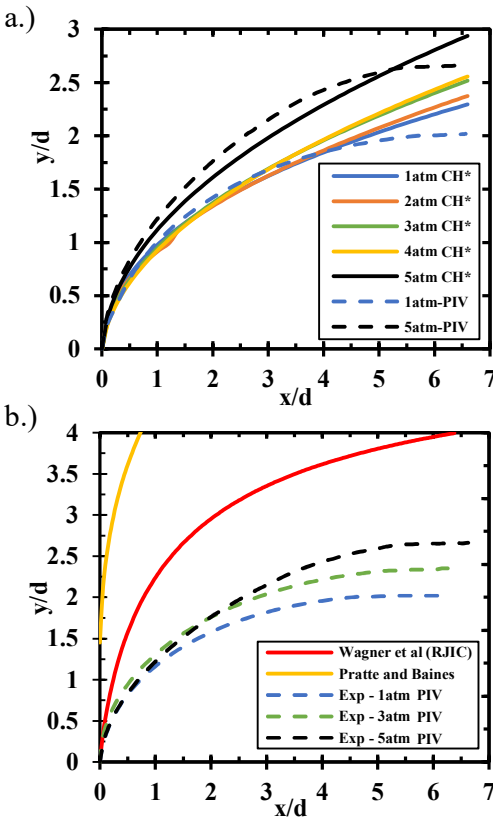

Fig. 6: (a) Experimental RJIC flame-based (CH*) and streamline-based (PIV) trajectories at various pressures, (b) Comparison of experimental PIV trajectories with correlations from the literature.

where *A*, *B*, *C* and *E* are constants and was developed for low momentum flux ranges, allowing a comparison with current work. Although the momentum flux of this study falls within the range used to develop the RJIC correlation, there is still a discrepancy between the trajectories, which is likely due to the higher turbulent conditions of the jet explored in the current work. It is noted that none of these correlations account for pressure effects.

$$Y = A\left(\frac{X^B}{X^B + E}\right) \tag{3}$$

Previous research has identified that jet trajectories are a function of entrainment and mixing characteristics [18, 28, 58], in which decreased crossflow entrainment was linked to increased jet penetration [26, 27]. Thus, pressure-driven variations of the jet trajectory are expected to be coupled with crossflow entrainment and mixing. At the higher pressures, the jet penetration was shown to increase, which can be associated to lower entrainment and mixing with the crossflow. One explanation for such behavior is the associated heat release of the flame upon the variation of pressure level. Heat release causes a change in the fluid density and velocity across the flame front, which results in a reduction of total entrained mass flow from the crossflow by the jet. The addition of heat release also drives a density gradient effect, which is experienced by the jet in the mixing layer. A "barrier" is formed between the jet core and the crossflow, resulting in a flame that is pushed further into the crossflow.

3.2. Flame Dispersion

The influence of pressure on the flame stabilization and growth is analyzed in this section. Utilizing the windward and leeward edges that were extracted from the CH* chemiluminescence data, the spread of the luminosity region (δ) was defined as the difference between the windward and leeward edge normal to the centerline. The spread of the jets for pressure cases 1, 3 and 5 are shown in Fig. 7a. The axial growth and width of the flame brush are dependent on entrainment rates, gas expansion, and momentum flux ratio [23, 26]. In this study, the momentum flux ratio is kept constant; thus, the key parameters driving the flame growth are the entrainment rates and thermal gas expansion of the jet at different pressure levels. There is a nearly linear growth for all cases as the axial distance from the jet increases, which can be linked to gas expansion.

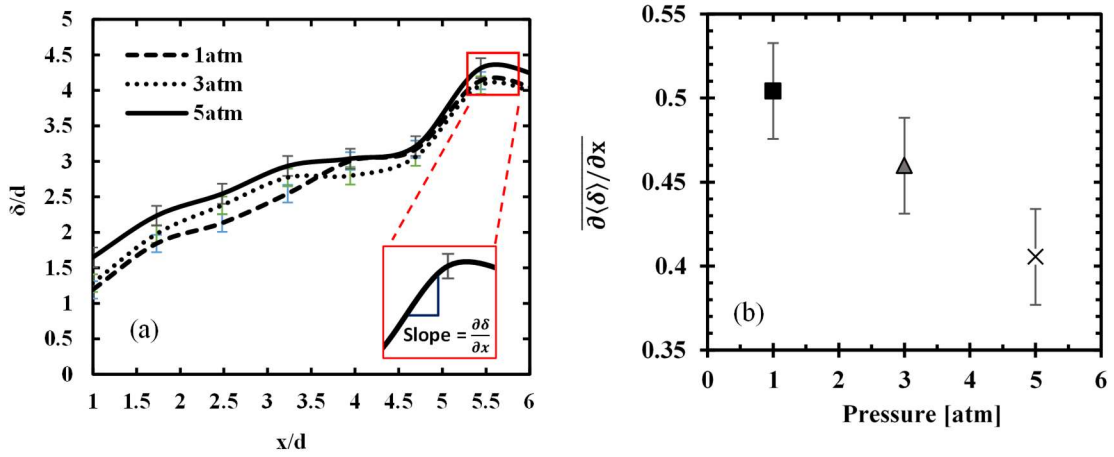

Fig. 7: (a) Flame brush spatial spread normal to the luminosity centerline. (b) Time average spatial rate of spread, error bars represent standard deviation from instantaneous flame edge and time average location.

In comparison to each other, the width of the reacting jet remains relatively constant at elevated pressure. The results from this section were also used to further understanding the time-averaged flame edge location, since it could vary due to the flapping of the jet. The change in width through the axial direction is shown in Fig 7b. This behavior agrees with the reacting jet in crossflow work presented by Sullivan et al. [55].

3.3. Flame Anchoring Point

The averaged CH* images were used to assess the flame liftoff height for all cases in this study. The flame liftoff height was determined using the stabilization point of the flame, which was defined as the nearest linear link between the jet exit and the flame (cf, fig, 3). An example is shown in fig. 4, represented with a cross symbol. The average transverse liftoff height is denoted as $\overline{y_{lgn}}$ and the average axial height is represented by $\overline{x_{lgn}}$. The average liftoff heights for the cases under pressure variation are shown in Fig. 8a. The findings suggest a dependency between pressure and flame liftoff. As pressure increases, both the transverse and axial liftoff height of the flame are seen to decrease

monotonically. Analyzing the 1 atm and 5 atm cases, there is a decrease of 20% in flame liftoff height. The stabilization point location fluctuated slightly for the higher-pressure condition. Further analysis was performed to correlate the flame stabilization location and ignition time scale τ_{ign}. The ignition time-scale was defined as the ratio between the average flame lift-off height and the jet velocity magnitude, as shown in Eq. (4) [55, 59].

$$\boldsymbol{\tau_{ign}} = \frac{\overline{\boldsymbol{LOH}}}{|\boldsymbol{u_j}|} \tag{4}$$

Figure 8b summarizes ignition delay time for all cases with a constant jet velocity. Uncertainty coupled to the jet stabilization vertical flapping is considered and represented as error bars. The results suggest a sensitivity of ignition time to pressure, similar to previous chemical kinetic research [60, 61]. The largest change occurs between the 1 atm and 3 atm cases, whereas a smaller variation can be seen at the higher-pressure cases. This suggests there is a nonlinear relationship between pressure and ignition of the mixture. The variation in ignition timescales can be associated with the faster chemical reaction rate and

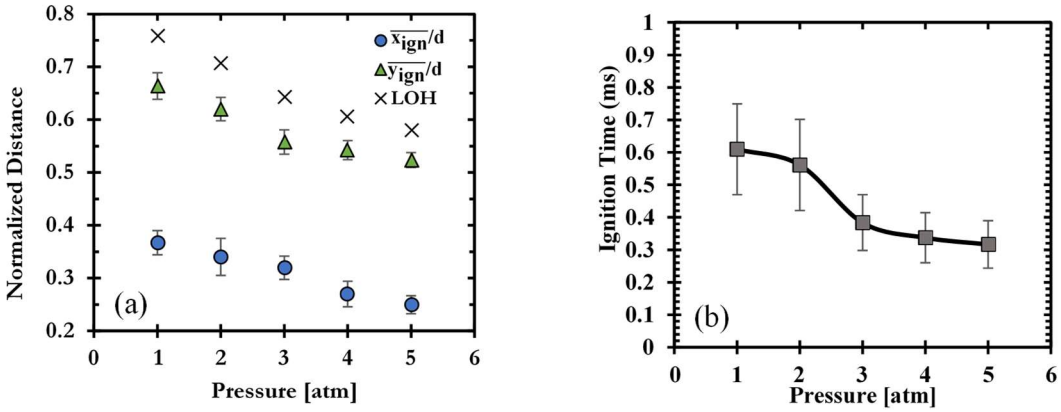

Fig. 8: (a) Flame liftoff height dependent on pressure, where x represents the liftoff height, defined as the closest point to the jet exit along the centerline. The axial and vertical displacement of the ignition point are shown as circles and triangles, respectively. (b) Ignition delay time for cases at different pressures; error bar represents standard deviation through time.

lower activation energy occurring at pressure. Due to the decrease of the ignition timescales and the flame liftoff, the data demonstrates the jet behavior to be largely influenced by the chemical timescales that change with pressure, compared to subordinate changes of the fluidic timescales, as shown in figs. 5 and 9.

3.4. Instantaneous Flame-Flow Interaction

Instantaneous span-wise vorticity (ω_z) and flame boundary are displayed in Fig. 9. The span-wise vorticity is normalized by the jet diameter and mean crossflow velocity, and presented as $\omega_z d_j/U$. It is noted that the overall field vorticity is nominally constant with pressure. However, an important distinction criterion are the relative locations of the flame-front and the shear vorticity. Shown in figure 10, the average vorticity along the flame

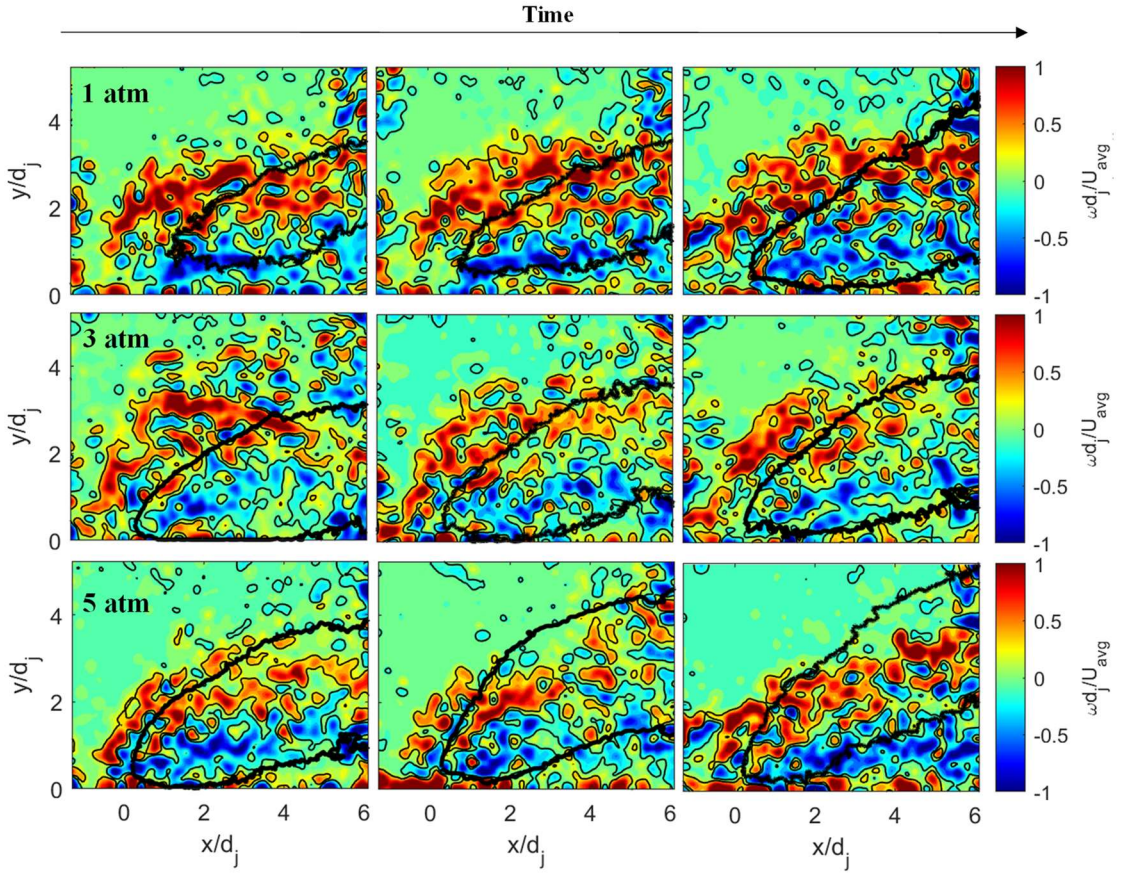

Fig. 9: Instantaneous flame brush overlay on normalized vorticity through time ($\omega d_j/U$).

boundary decreases in magnitude with pressure. Since vorticity is associated with fluid rotation, the decrease in vorticity magnitudes at elevated pressures will be linked to increased (slower) fluidic and mixing timescales. From a Damköhler number perspective ($Da = \tau_{flow}/\tau_{chem}$), elongating the fluid timescales while decreasing the chemical timescales will provide favorable ignition conditions with elevated pressure. The increase in fluid timescales and the decrease in reaction rate, indicate an increase of the Damköhler number with pressure [62]. This causes the flame liftoff height and ignition delay time to both decrease, as previously depicted in Fig. 8. These results are also consistent with previous work, which suggests that elevated strain rates near the RJIC inhibit flame stabilization and increase liftoff heights [29]. Essentially, regions with low strain rates (or low vorticity magnitudes) provide a dynamic balance between the flame speed and the flow, and the reaction can be sustained. The higher vorticity seen at ambient pressure implies higher strain rate experienced along the shear layer. This higher strain rate can inhibit the fluid to ignite due to shorter mixing time scale. Moving downstream from the jet exit, the vorticity gradient decreases for the lower pressure jet, allowing the fluid to ignite.

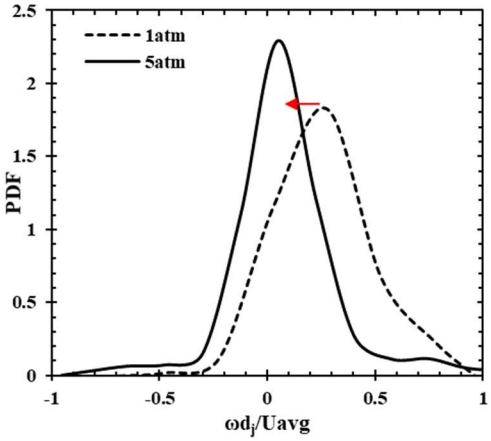

Fig. 10: Probability density function (pdf) of normalized vorticity extracted from PIV at the averaged windward edge of flame.

For all the cases, the jet shows to stabilize initially on the leeward side of the recirculation zone. This behavior is expected due to the lower velocity in the area which allows the jet to sustain itself with combustion products from the jet wake. However, some variations are seen among the different pressure cases. The higher-pressure flames show to

stabilize closer to the jet exit due to the lower vorticity around the jet. As the pressure increases, the jet flames are seen to shift from a shear layer burning to a core burning flame. The flame stabilization at the shear layer region most likely is driven by autoignition at the leeward side and propagates to the windward edge. For the cases at higher pressures, the flame stabilizes at the center of the jet (away from the shear layer), suggesting a shift from autoignition flame stabilization to a premixed flame propagation mechanism. This most likely indicates that the reactants consumed are solely from the jet mixture, since there is a lack of mixing from the crossflow.

3.5. Emissions

Emissions data for the axially staged combustor was obtained over the range of pressure conditions previously discussed (Table 1). In order to evaluate the emissions benefit gained from an axially staged combustor, emissions data were obtained with the staged combustor relative to a single staged system. A schematic depicting the emissions measurement locations is provided in Fig. 11. For the single stage combustor, all fuel and air are burned in one combustor. In contrast, only a portion of the fuel is initially burned in the staged combustor, and the remaining fuel and oxidizer are burned in the secondary (axial) stage.

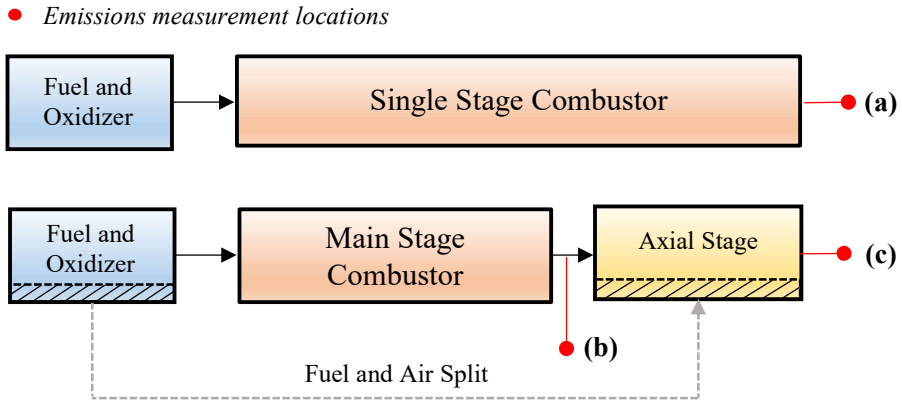

Fig. 11: Schematic of emissions measurements location: (a) Outlet of single stage combustor. (b) Outlet of main stage combustor. (c) Outlet of axially staged combustor.

For all conditions, emissions measurements were obtained at the outlet of the main burner (prior to the axial stage), at the exit of the staged facility, and at the outlet of a global single stage facility, to quantify the NOx reduction potential of the staged architecture. Main burner emission levels (fig. 12 (a) blue curve) were obtained along with second stage exit emission data (fig. 12 (b) blue curve) and their difference is shown in fig. 12 (c). To relate the trends recorded for pressure vs. NOx emission with the staged configuration, the same conditions were tested in the single stage configuration (fig. 12 (a) and (b) orange curve), combusting the similar total amount of fuel in one stage. These NOx emission data scale approximately with $X(NO_x) = f(p^{0.5})$ and show to match with the trends found in the literature [50]. As pressure increases, NOx levels

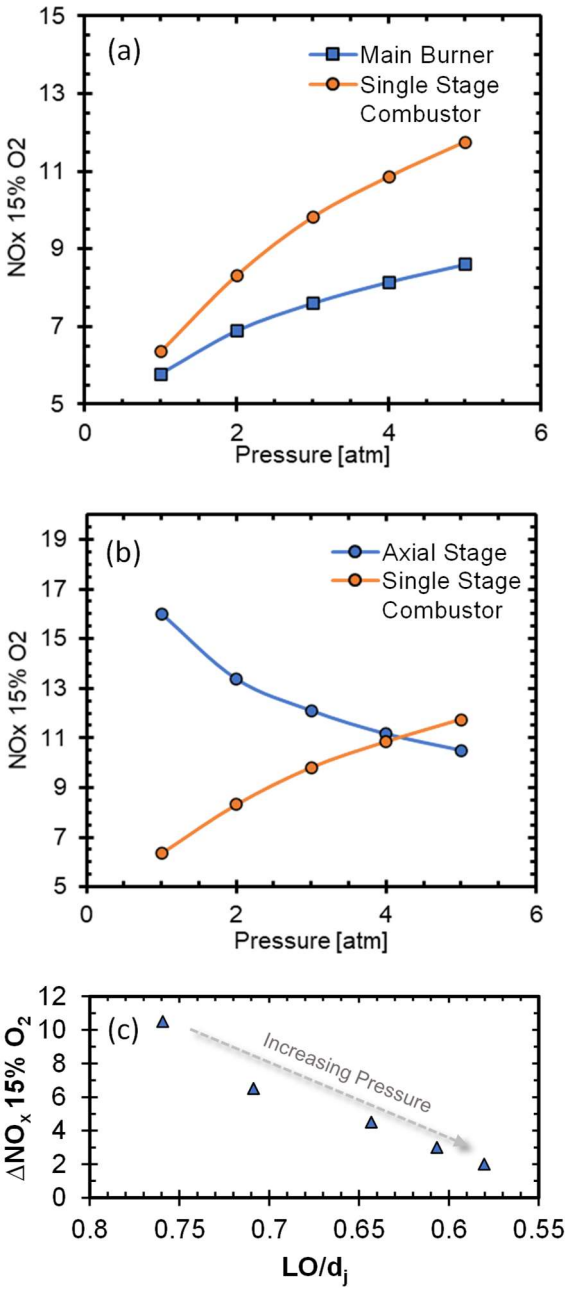

Fig. 12: NO_x emissions vs. pressure (a) comparison between a single stage combustion system and the first stage of an axially staged combustor (main burner). (b) Comparison between a single stage combustor and the axial stage combustor outlet (global outlet). (c) NO_x contribution of the axial stage for the staged combustor configuration, this curve is obtained from the subtraction of (a) – (b).

of any main burner/single stage configuration would increase as well. Due to the reduced fuel amount combusted in the first burner stage, emission levels were reduced relative to a single staged configuration. Figure 12 (b) demonstrates the corrected NOx levels for the axial stage and compared to the single stage emission. The global outlet emission data shows a reduction of NOx due to the axially staged configuration, which is the inverse trend relative to the single stage configuration. The single stage emissions indicate an increase at pressure while the emissions level from the axial stage show to inversely decrease with pressure, which is a novel finding investigated for the pressure range between 1atm and 5atm within these studies. The axial stage emission outlet trend was determined to be $X(NO_x) = f(p^{-0.55})$ by [62]. In a conventional gas turbine combustor, NOx levels increase with pressure, a behavior that is altered in the jet-in-crossflow stage due to the specific characteristics in the flow field and flame parameters at pressure. As stated previously, pressure influences the balance between chemical and fluid mechanical timescales, which induces changes to the flame liftoff, dispersion, and stabilization mechanism. It was reported [62] that the RJIC transitions from shear burning to core burning with the onset of elevated pressure, which is the driving mechanism for the decrease of axial NOx levels. Numerical studies on the similar condition by [62] suggested the 5atm operating point to burn as a compact flame, limiting the high temperature local regions between the crossflow and the jet as well as the flame surface along the shear layer.

Finally, ΔNOx was calculated to isolate the net NOx addition in the secondary stage (fig. 12 (c)). ΔNOx represents the difference between the emissions from the staged main burner and the emissions obtained from the facility exit downstream of the axial stage (global outlet). As pressure increases, the flame liftoff is decreased, and there is a

subsequent decrease in ΔNOx. In other words, the NOx benefit from axial staging becomes significantly more prevalent at elevated pressure. This demonstrates an underestimation of NOx production relative to previous research reported for atmospheric conditions. This research emphasizes the value of providing data at elevated pressure to industry, which provides more practical knowledge to aid combustor development.

4. CONCLUSION

The work in this study investigates the influence of pressure on the flame characteristics of a premixed reacting jet injected into a lean vitiated at a pressure range between 1 and 5 atmospheres. The increase in the combustor pressure altered the trajectories of the flow field and the flame, and increased jet penetration was observed at elevated pressure. Increasing the pressure also altered the flame stabilization process, and the ignition timescales were shown to decrease with elevated pressure.

To discern the source of decreased ignition timescales, the flame and flow field was investigated for various pressure conditions. The bulk flow field was nominally constant with pressure, which suggests that the variations of the ignition timescales were primarily attributed to chemical effects, rather than driven by fluid mechanics. Although the flow field remained nominally unchanged, the position of the flame with respect to the vorticity field was pushed further outward, beyond the windward shear, layer at higher pressure. The change to the global flame position suggests that turbulence-flame interactions and local flame Damköhler number are altered at elevated pressure. This was validated by quantifying the local vorticity along the windward flame branch, which decreased with elevated pressure. This is indicative of slower fluid mechanical timescales, which, as they

are coupled with decreased chemical timescales, can provide more favorable conditions for the flame to stabilize at elevated pressure levels.

Concurrently, NOx emissions measurements were obtained for the pressure range of 1-5 atm. The measurements demonstrate that the NOx contribution from the axial stage decreases with elevated pressure. This measured emission reduction potential was shown to outweigh the single staged combustor configuration at elevated pressure level, while the lift-off was decreased. The results of this work demonstrate a relationship between pressure and flame liftoff, which is considered a driving parameter for NOx production. Future work could potentially include more parameters to study a larger range of momentum flux and axial equivalence ratio, to expand on the relationship of the effect of pressure on the fluidic and chemical time scales.

ACKNOWLEDGMENTS

The authors (MO, TG, BS, AM, KA and SM) acknowledge support from the Department of Energy under Award Number DE-FE0031227 and collaboration with Dr. Changjin Yoon and GE Global Research.

necessarily constitute or imply its endorsement, recommendation, or favoring by the United States Government or any agency thereof. The views and opinions of authors expressed herein do not necessarily state or reflect those of the United States Government or any agency thereof.

References

[1] Berkley Davis, L., *Dry Low NOx Combustion Systems for GE Heavy-Duty Gas Turbines*.

[2] Leonard, G., and Stegmaier, J., 1994, "Development of an Aeroderivative Gas Turbine Dry Low Emissions Combustion System," J. Eng. Gas Turbines Power, **116**(3), pp. 542–546.

[3] Prade, B., 2013, "Gas Turbine Operation and Combustion Performance Issues," *Modern Gas Turbine Systems*, Elsevier, pp. 383-423e.

[4] Rizk, N. K., Mongia, H. C., Gas, A., Division, T., and Corporation, G. M., 1990, "Ultra-Low NOx Rich-Lean Combustion," Am. Soc. Mech. Eng.

[5] Rizk, N. K., and Mongia, H. C., 1991, "Lean Low NOx Combustion Concept Evaluation," Symp. Combust., **23**(1), pp. 1063–1070.

[6] Zeldovich, I., Barenblatt, G., and Librovich, V., 1985, *Mathematical Theory of Combustion and Explosions*.

[7] Zevenhoven, R, Kilpinen, P., 2001, "Control of Pollutants in Flue Gases and Fuel Gases," pp. 73–136.

[8] Correa, S. M., 1993, "A Review of NO x Formation Under Gas-Turbine Combustion Conditions," Combust. Sci. Technol., **87**(1–6), pp. 329–362.

[9] Thompson, D., Brown, T. D., and Beér, J. M., 1972, "NOx Formation in Combustion," Combust. Flame, **19**(1), pp. 69–79.

[10] Sullivan, D. A., 1977, "A Simple Gas Turbine Combustor NOx Correlation Including the Effect of Vitiated Air," J. Eng. Power, **99**(2), pp. 145–152.

[11] Rutar, Teodora, Martin, Scott, Nicol, D., "An Engineering Modeling Study of NOx Dependency on Incomplete Premixing at Gas Turbine Engine Conditions."

[12] Sattelmayer, T., Polifke, W., Winkler, D., and Döbbeling, K., 1998, "Nox-Abatement Potential of Lean-Premixed GT Combustors," J. Eng. Gas Turbines Power, **120**(1), pp. 48–59.

[13] Nicol, D., Malte, P. C., Lai, J., Marinov, N. N., Pratt, D. T., and Corr, R. A., 1992, "NOx Sensitivities for Gas Turbine Engines Operated on Lean-Premixed Combustion and Conventional Diffusion Flames," *Volume 3: Coal, Biomass and Alternative Fuels; Combustion and Fuels; Oil and Gas Applications; Cycle Innovations*, American Society of Mechanical Engineers.

[14] Winkler, D., Geng, W., Engelbrecht, G., Stuber, P., Knapp, K., and Griffin, T., 2017, "Staged Combustion Concept for Gas Turbines," J. Glob. Power Propuls. Soc., **1**, p. CVLCX0.

[15] Karim, H., Natarajan, J., Narra, V., Cai, J., Rao, S., Kegley, J., and Citeno, J., 2017, "Staged Combustion System for Improved Emissions Operability and Flexibility for 7HA Class Heavy Duty Gas Turbine Engine," *Proceedings of ASME Turbo Expo: Power for Land, Sea and Air*, American Society of Mechanical Engineers, pp. 1–10.

[16] Martin, S. M., Laster, W. R., and Bilbao, J. E. P., 2017, "Axial Stage Combustion System with Exhaust Gas Recirculation."

[17] Lefebvre, A. H., and Ballal, D. R., 2010, *Gas Turbine Combustion: Alternative Fuels and Emissions*.

[18] Karagozian, A. R., 2010, "Transverse Jets and Their Control," Prog. Energy Combust. Sci., **36**(5), pp. 531–553.

[19] Mahesh, K., 2013, "The Interaction of Jets with Crossflow," Annu. Rev. Fluid Mech., **45**(1), pp. 379–407.

[20] D-, N. T. N., and Holdeman, J. D., 1972, "Correlation for Temperature Profiles in the Plane of Symmetry Downstream of a Jet Injected Normal to a Crossflow," Security, (September).

[21] Becker, H. A., and Yamazaki, S., 1978, "Entrainment, Momentum Flux and Temperature in Vertical Free Turbulent Diffusion Flames," Combust. Flame, **33**(C), pp. 123–149.

[22] Pratte, B. D., and Baines, W. D., 1967, "Profiles of the Round Turbulent Jet in A Cross Flow."

[23] Hasselbrink, E. F., and Mungal, M. G., 2001, "Transverse Jets and Jet Flames. Part 1. Scaling Laws for Strong Transverse Jets," J. Fluid Mech., **443**, pp. 1–25.

[24] Yao, T., Yang, W. H., and Luo, K. H., 2018, "Direct Numerical Simulation Study of Hydrogen/Air Auto-Ignition in Turbulent Mixing Layer at Elevated Pressures,"

Comput. Fluids, **173**, pp. 59–72.

[25] Steinberg, A. M., Sadanandan, R., Demb, C., Kutne, P., and Meier, W., 2013, "Structure and Stabilization of Hydrogen Jet Flames in Cross-Flows," Proc. Combust. Inst., **34**(1), pp. 1499–1507.

[26] Hasselbrink, E. F., and Mungal, M. G., 2001, "Transverse Jets and Jet Flames. Part 2. Velocity and OH Field Imaging," **443**, pp. 27–68.

[27] Hasselbrink, E. F., and Mungal, M. G., 1996, "An Analysis of the Time-Averaged Properties of the Far Field of the Transverse Jet," 34th Aerosp. Sci. Meet. Exhib., (January).

[28] Ricou, F. P., and Spalding, D. B., 1961, "Measurements of Entrainment by Axisymmetrical Turbulent Jets," J. Fluid Mech., **11**(1), pp. 21–32.

[29] Wagner, J. A., Dayton, J. W., Linevitch, K., and Cetegen, B. M., 2018, "Flame Stabilization of a Premixed Reacting Jet in Vitiated Crossflow," Proc. Combust. Inst., **36**(3), pp. 3763–3771.

[30] Nair, V., Sirignano, M., Emerson, B., Halls, B., Jiang, N., Felver, J., Roy, S., Gord, J., and Lieuwen, T., 2019, "Counter Rotating Vortex Pair Structure in a Reacting Jet in Crossflow," Proc. Combust. Inst., **37**(2), pp. 1489–1496.

[31] Rodrigues, N. S., Busari, O., Senior, W. C. B., McDonald, C. T., Chen, Y. T., North, A. J., Laster, W. R., Meyer, S. E., and Lucht, R. P., 2020, "NOX Reduction in an Axially Staged Gas Turbine Model Combustor through Increase in the Combustor Exit Mach Number," Combust. Flame, **212**(X), pp. 282–294.

[32] Pinchak, M. D., Shaw, V. G., and Gutmark, E. J., 2018, "The Effects of Nozzle Geometry and Equivalence Ratio on a Premixed Reacting Jet in Vitiated Cross-Flow," Combust. Flame, **191**, pp. 353–367.

[33] Saini, P., Chterev, I., Pareja, J., Aigner, M., and Boxx, I., 2020, "Effect of Pressure on Hydrogen Enriched Natural Gas Jet Flames in Crossflow," Flow, Turbul. Combust., **105**(3), pp. 787–806.

[34] Meyer, K. E., Pedersen, J. M., and Özcan, O., 2007, "A Turbulent Jet in Crossflow Analysed with Proper Orthogonal Decomposition," J. Fluid Mech., **583**(2007), pp. 199–227.

[35] Zerhouni, E., 2006, "Clinical Research at a Crossroads: The NIH Roadmap.," J. Investig. Med., **54**(4), pp. 171–173.

[36] Bandaru, R. V., and Turns, S. R., 2000, "Turbulent Jet Flames in a Crossflow: Effects of Some Jet, Crossflow, and Pilot-Flame Parameters on Emissions," Combust. Flame, **121**(1–2), pp. 137–151.

[37] Lamont, W. G., Roa, M., Meyer, S. E., and Lucht, R. P., 2012, "Emission Measurements and CH* Chemiluminescence of a Staged Combustion Rig for Stationary Gas Turbine Applications," J. Eng. Gas Turbines Power, **134**(8), pp. 1–8.

[38] Kolb, M., Ahrens, D., Hirsch, C., and Sattelmayer, T., 2016, "A Model for Predicting the Lift-off Height of Premixed Jets in Vitiated Cross Flow," J. Eng. Gas Turbines Power, **138**(8), pp. 1–9.

[39] Wagner, J. A., Grib, S. W., Renfro, M. W., and Cetegen, B. M., 2015, "Flowfield Measurements and Flame Stabilization of a Premixed Reacting Jet in Vitiated Crossflow," Combust. Flame, **162**(10), pp. 3711–3727.

[40] Ebi, D., Doll, U., Schulz, O., Xiong, Y., and Noiray, N., 2019, "Ignition of a Sequential Combustor : Evidence of Flame Propagation in the Autoignitable Mixture," Proc. Combust. Inst., **37**, pp. 5013–5020.

[41] Ahrens, D., Kolb, M., Hirsch, C., and Sattelmayer, T., 2014, "NOx Formation in a Reacting Premixed Jet in Hot Cross Flow," *Volume 4B: Combustion, Fuels and Emissions*, American Society of Mechanical Engineers, pp. 1–13.

[42] Goh, E., Sirignano, M., Nair, V., Emerson, B., Lieuwen, T., and Seitzman, J., 2017, "Modeling of Minimum NOx in Staged-Combustion Architectures at Elevated Temperatures," *Proceedings of the ASME Turbo Expo*, pp. 1–8.

[43] Roa, M., Lamont, W. G., Meyer, S. E., Szedlacsek, P., and Lucht, R. P., 2012, "Emission Measurements and Oh-Plif of Reacting Hydrogen Jets in Vitiated Crossflow for Stationary Gas Turbines," *Proceedings of the ASME Turbo Expo*, pp. 491–498.

[44] Prathap, C., Galeazzo, F. C. C., Kasabov, P., Habisreuther, P., Zarzalis, N., Beck, C., Krebs, W., and Wegner, B., 2012, "Analysis of NOX Formation in an Axially Staged Combustion System at Elevated Pressure Conditions," J. Eng. Gas Turbines Power, **134**(3), p. 031507.

[45] Lyle, K. H., Tseng, L. K., Gore, J. P., and Laurendeau, N. M., 1999, "A Study of Pollutant Emission Characteristics of Partially Premixed Turbulent Jet Flames," Combust. Flame, **116**(4), pp. 627–639.

[46] Rutar, T., and Malte, P. C., 2002, "Nox Formation in High-Pressure Jet-Stirred Reactors with Significance to Lean-Premixed Combustion Turbines," J. Eng. Gas Turbines Power, **124**(4), pp. 776–783.

[47] Sirignano, M. D., Nair, V., Emerson, B. L., Seitzman, J., and Lieuwen, T. C., 2020, "Nitrogen Oxide Emissions from Premixed Reacting Jets in a Vitiated Crossflow," Combust. Sci. Technol., **192**(7), pp. 1389–1419.

[48] Steele, R. C., Tonouchi, J. H., Nicol, D. G., Horning, D. C., Malte, P. C., and Pratt, D. T., 1998, "Characterization of NOx, N20, and CO for Lean-Premixed Combustion in a High-Pressure Jet-Stirred Reactor," J. Eng. Gas Turbines Power, **120**(2), pp. 303–310.

[49] Han, D. S., Kim, G. B., Kim, H. S., and Jeon, C. H., 2014, "Experimental Study of NOx Correlation for Fuel Staged Combustion Using Lab-Scale Gas Turbine Combustor at High Pressure," Exp. Therm. Fluid Sci., **58**(x), pp. 62–69.

[50] Biagioli, F., and Güthe, F., 2007, "Effect of Pressure and Fuel-Air Unmixedness on NOx Emissions from Industrial Gas Turbine Burners," Combust. Flame, **151**(1–2), pp. 274–288.

[51] Hoferichter, V., Ahrens, D., Kolb, M., and Sattelmayer, T., 2014, "A Reactor Model for the Nox Formation in a Reacting Jet in Hot," *Proceedings of ASME Turbo Expo*, pp. 1–10.

[52] Thielicke, W., and Stamhuis, E. J., 2014, "PIVlab – Towards User-Friendly, Affordable and Accurate Digital Particle Image Velocimetry in MATLAB," J. Open Res. Softw., **2**.

[53] He, K., Sun, J., and Tang, X., 2013, "Guided Image Filtering," IEEE Trans. Pattern Anal. Mach. Intell., **35**(6), pp. 1397–1409.

[54] Otsu, N., 1979, "A Threshold Selection Method from Gray-Level Histograms," IEEE Trans. Syst. Man. Cybern., **9**(1), pp. 62–66.

[55] Sullivan, R., Wilde, B., Noble, D. R., Seitzman, J. M., and Lieuwen, T. C., 2014, "Time-Averaged Characteristics of a Reacting Fuel Jet in Vitiated Cross-Flow," Combust. Flame, **161**(7), pp. 1792–1803.

[56] Smith, S. H., and Mungal, M. G., 1998, "Mixing, Structure and Scaling of the Jet in Crossflow," J. Fluid Mech., **357**, pp. 83–122.

[57] Pratte, B., 1967, "Profiles of the Round Turbulent Jet in A Cross Flow," J. Hydraul. Div., **93**(6).

[58] Mungal, M. G., and Hasselbrink, E. F., 2003, "Jets in Crossflow — Effects of Heat Release," pp. 173–182.

[59] Wagner, J. A., Grib, S. W., Renfro, M. W., and Cetegen, B. M., 2015, "Flowfield Measurements and Flame Stabilization of a Premixed Reacting Jet in Vitiated Crossflow," Combust. Flame, **162**(10), pp. 3711–3727.

[60] Hu, E., Li, X., Meng, X., Chen, Y., Cheng, Y., Xie, Y., and Huang, Z., 2015, "Laminar Flame Speeds and Ignition Delay Times of Methane-Air Mixtures at Elevated Temperatures and Pressures," Fuel, **158**, pp. 1–10.

[61] Norrish, R.G.W, Foord, S. ., 1936, “The Kinetics of the Combustion of Methane,” Proc. R. Soc. London. Ser. A - Math. Phys. Sci., **157**(892), pp. 503–525.

[62] Stiehl, B., Otero, M., Genova, T., Martin, S., and Ahmed, K., 2021, "The Effect of Pressure on NO_x Entitlement and Reaction Timescales in a Premixed Axial Jet-In-Crossflow." ASME. J. Energy Resour. Technol. **143**(11)